

Holistic genetic optimization of a Generalized Multiple Discrete Interaction Approximation for wind waves [☆]



Hendrik L. Tolman ^{*}, Robert W. Grumbine

NOAA/NCEP/EMC, Marine Modeling and Analysis Branch, 5830 University Research Court, College Park, MD 20740, USA

ARTICLE INFO

Article history:

Available online 20 January 2013

Keywords:

Wind waves
Resonant nonlinear interactions
Discrete interaction approximation
Genetic optimization

ABSTRACT

A key element of wind wave models is the parameterization of the resonant nonlinear interactions between spectral wave components. In a companion paper a new Generalized Multiple Discrete Interaction Approximation (GMD) has been developed. The present paper addresses the optimization of the free parameters of the GMD. A holistic optimization approach is used where full model integration results are optimized. Fifteen objective metrics are used, defined to measure the accuracy of a model using the GMD relative to a model using the full (exact) interactions. Due to the large number of free parameters to be optimized, and due to the existence of many local error minima in parameter space, traditional error mapping or steepest descent search algorithms are not suitable to optimize the GMD. The focus of the present study is on establishing genetic optimization techniques as a feasible and economical way to optimize the free parameters in the GMD. The behavior of the GMD with optimized parameters is outside the scope of this study, and is discussed in detail in the companion paper.

Published by Elsevier Ltd.

1. Introduction

Modeling of wind waves at sea and on other water bodies generally considers the evolution of their energy or variance spectrum. Traditionally, such a spectrum F is a density function defined in terms of a spectral frequency f and a spectral direction θ , and ignores the phase of spectral components. This spectrum $F(f, \theta)$ deterministically describes the statistical properties of the wind waves. In its most elementary form, the evolution equation for this spectrum can be described using a balance equation (e.g., Hasselmann, 1960)

$$\frac{DF(f, \theta)}{Dt} = S_{in} + S_{nl} + S_{ds} + \dots, \quad (1)$$

where the left side represents linear wave propagation, and the right side represents sources and sinks of wave energy, consisting of wind input (S_{in}), nonlinear interactions (S_{nl}), dissipation (S_{ds}), and additional processes, typically associated with shallow water. In these source terms, the nonlinear interactions play a central role. They represent the lowest order process known to move energy to lower frequencies, increasing the dominant wave length as is observed during wave growth. Furthermore, they stabilize the spectral shape at high frequencies (e.g., Hasselmann, 1973). The SWAMP study (SWAMP Group, 1985) identified the need for fully computing the nonlinear interactions in wave models (instead of parameteriz-

ing the effects of the interactions). Such models are generally denoted as third-generation wave models.

The nonlinear interactions describe the resonant (conservative) exchange of energy, action and momentum between four wave components that satisfy the resonance conditions

$$\mathbf{k}_1 + \mathbf{k}_2 = \mathbf{k}_3 + \mathbf{k}_4, \quad (2)$$

$$\sigma_1 + \sigma_2 = \sigma_3 + \sigma_4, \quad (3)$$

where \mathbf{k} is the wavenumber vector with magnitude k and direction θ , and where $\sigma = 2\pi f$ is the intrinsic wave frequency. Such a combination of four waves is generally referred to as a quadruplet. Computation of the full nonlinear interactions requires the integration of a six-dimensional Boltzmann integral. Although much progress has been made in optimizing the computation of the full nonlinear interactions (e.g., Van Vledder, 2006), they are still several orders of magnitude too expensive for the use in operational wave models.

Third generation wave models became feasible with the development of the Discrete Interaction Approximation (DIA, Hasselmann et al., 1985). In this approximation, the multi-dimensional Boltzmann integral is replaced by evaluating interaction contributions locally in spectral space for representative quadruplets only. The representative quadruplet is defined by the resonance conditions (2) and (3), and by

$$\left. \begin{aligned} \mathbf{k}_1 &= \mathbf{k}_2 \\ \sigma_3 &= (1 + \lambda)\sigma_1 \\ \sigma_4 &= (1 - \lambda)\sigma_1 \end{aligned} \right\}, \quad (4)$$

[☆] MMAB contribution Nr. 308.

^{*} Corresponding author. Tel.: +1 301 683 3748; fax: +1 301 683 3701.

E-mail address: Hendrik.Tolman@NOAA.gov (H.L. Tolman).

for which the contributions to the source term at the four components of the quadruplet are computed as

$$\begin{pmatrix} \delta S_{nl,1} \\ \delta S_{nl,3} \\ \delta S_{nl,4} \end{pmatrix} = \begin{pmatrix} -2 \\ 1 \\ 1 \end{pmatrix} C g^{-4} f_1^{11} \times \left[F_1^2 \left(\frac{F_3}{(1+\lambda)^4} + \frac{F_4}{(1-\lambda)^4} \right) - \frac{2F_1 F_3 F_4}{(1-\lambda^2)^4} \right], \quad (5)$$

where $F_i = F(f_i, \theta_i)$ represent the spectral energy density at the four components of the quadruplets, and $\delta S_{nl,i} = \delta S_{nl}(f_i, \theta_i)$ are the corresponding contributions to the interactions. λ and C are free parameters in this parameterization, set to $\lambda = 0.25$ and $C = 3 \times 10^7$ by Hasselmann et al. (1985).

Whereas the DIA made operational third generation wave models feasible, it was recognized from its inception as having limited accuracy. Since then, many attempts have been made to develop more accurate yet economical parameterizations for the nonlinear interactions. A recent review can be found in the companion paper (Tolman, accepted for publication). The latter paper presents a Generalized Multiple DIA (GMD) which represents an expansion on the traditional DIA, with several additional features.¹

First, a more flexible definition for the representative quadruplet is introduced by expanding Eq. (4) to

$$\begin{cases} \sigma_1 = (1 + \mu)\sigma \\ \sigma_2 = (1 - \mu)\sigma \\ \sigma_3 = (1 + \lambda)\sigma \\ \sigma_4 = (1 - \lambda)\sigma \end{cases}, \quad (6)$$

with free parameters λ and μ , reducing to the one-parameter definition for $\mu = 0$. Furthermore, it can be expanded to a three-parameter definition by defining the internal angle θ_{12} between quadruplet components 1 and 2 as an additional free parameter. The three-parameter definition reduces to (4) for $\mu = 0$ and $\theta_{12} = 0^\circ$.

Second, the GMD quadruplets are evaluated at the actual depth, whereas in the DIA all quadruplets are evaluated assuming deep water. This is essential to assure that the GMD reproduces all conservation properties of the exact interactions.

Third, multiple representative quadruplets are allowed, with their individual contributions to the interactions normalized so that the interactions computed for multiple copies of the same representative quadruplet are identical to interactions computed from one such representative quadruplet.

Fourth, the GMD features complementary scaling for weak interactions in deeper water ($kd > 0.50$, consistent with the interactions described in the DIA), and strong interactions as occur in extremely shallow water ($kd < 0.75$, not reproduced by the DIA).

With these expansions, contributions to the interactions from a single quadruplet realization in the GMD become

$$\begin{pmatrix} \delta S_{nl,1} \\ \delta S_{nl,2} \\ \delta S_{nl,3} \\ \delta S_{nl,4} \end{pmatrix} = \begin{pmatrix} -1 \\ -1 \\ 1 \\ 1 \end{pmatrix} \left(\frac{1}{n_{q,d}} C_{\text{deep}} B_{\text{deep}} + \frac{1}{n_{q,s}} C_{\text{sh}} B_{\text{sh}} \right) \times \left[\frac{c_{g,1} F_1}{k_1 \sigma_1} \frac{c_{g,2} F_2}{k_2 \sigma_2} \left(\frac{c_{g,3} F_3}{k_3 \sigma_3} + \frac{c_{g,4} F_4}{k_4 \sigma_4} \right) - \frac{c_{g,3} F_3}{k_3 \sigma_3} \frac{c_{g,4} F_4}{k_4 \sigma_4} \left(\frac{c_{g,1} F_1}{k_1 \sigma_1} + \frac{c_{g,2} F_2}{k_2 \sigma_2} \right) \right], \quad (7)$$

where the scaling functions B_{deep} for weak interactions and $B_{\text{sh}} for strong interactions are defined as$

$$B_{\text{deep}} = \frac{k^{4+m} \sigma^{13-2m}}{(2\pi)^{11} g^{4-m} c_g^2}, \quad (8)$$

$$B_{\text{sh}} = \frac{g^2 k^{11}}{(2\pi)^{11} c_g} (kd)^n, \quad (9)$$

where m and n are tunable parameters, $n_{q,d}$ and $n_{q,s}$ are the number of representative quadruplets describing weak and strong interactions, respectively, and C_{deep} and C_{sh} are the corresponding proportionality constants.

The traditional DIA only has two free parameters, λ and C . The GMD has many more free parameters. There are n_q representative quadruplets with up to five free parameters per quadruplet ($\lambda, \mu, \theta_{12}, C_{\text{deep}}, C_{\text{sh}}$), as well as two free parameters in the scaling function (m, n). The present study focuses on efficient ways to optimize these free parameters. The two distinct aspects of the optimization techniques used here are holistic and genetic optimization. Holistic optimization implies that results of full wave model integrations are optimized, instead of optimizing nonlinear interactions for test spectra only. The holistic optimization approach is described in Section 2. Genetic optimization is used here to efficiently optimize a large number of free parameters while dealing with many local error minima in parameters space, and with discontinuous error behavior in parameter space (as will be illustrated below in Fig. 1b). The basic principles of genetic optimization are described in Section 3, and a full description is presented in Appendix B.

The new optimization techniques are described and illustrated here by considering deep water conditions only, where C_{sh}, m and n are not optimized. Application of these techniques to shallow water follow similar principles, and are presented in Tolman (2010a). Results are presented in Section 4. A discussion and conclusions are presented in Section 5.

2. Holistic optimization

Holistic optimization is not new to nonlinear interactions in wind waves. Hasselmann et al. (1985) based their parameter estimates for the DIA on full wave model runs, but used subjective error measures. Since then, most interaction studies have considered evaluating interactions for test spectra only. Tolman et al. (2004) and Tolman (2005) reintroduced holistic optimization, as it became evident that more accurate fitting of interactions to test spectra is no guarantee for better wave model behavior, or even for stable model integration.

Development, optimization and validation of interaction parameterizations requires evaluation of exact interactions. In this study exact interactions are computed using the Webb–Resio–Tracy (WRT) method (Webb, 1978; Tracy and Resio, 1982; Resio and Perrie, 1991), as implemented in the portable package developed by Van Vledder (2002, 2006).²

Holistic optimization of nonlinear interactions requires the adoption of a full wind wave model. In this study research version 3.15 of WAVEWATCH III[®] has been used. For all practical purposes, this model is identical to the recently released model version 3.14 (Tolman, 2009). This model includes the above identified WRT package for exact interactions, the traditional DIA, and the GMD. With the exception of the choice of nonlinear interactions, default settings of this model are used. To assure sufficient spectral resolution for WRT computations, the spectra are discretized using 36 directions ($\Delta\theta = 10^\circ$) and a relative frequency increment of 7%, with a discrete spectral frequency range as recommended by Van Vledder (2006) (0.04–0.78 Hz for the tests considered here).

¹ Additional information on the GMD can be found in the reports Tolman (2008, 2010a).

² Model version 5.04 used here.

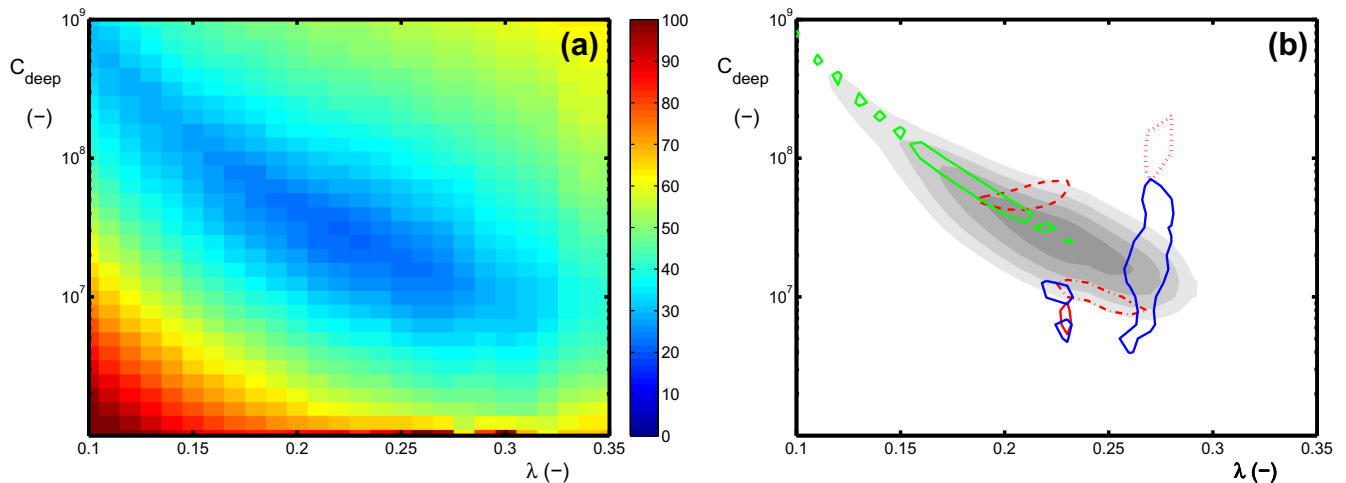


Fig. 1. Error mapping in $(\lambda, C_{\text{deep}})$ parameter space for a traditional DIA configuration of the GMD. (a) Total error in percent for all combined deep water tests. (b) Composite of optimum error regions; gray shaded area is total error at 10% increments above minimum error. Contour lines represent minimum error + 10% for individual parameters; H_s : red chain line, f_p : red dashed line, $\bar{\theta}$: red dotted line, σ_θ : red solid line; β : green lines; $\theta(f)$ blue lines. (For interpretation of the references to colour in this figure legend, the reader is referred to the web version of this article.)

The holistic optimization requires test cases, test parameters and error metrics, as discussed in the following sections.

2.1. Test cases

Test cases need to be simple and cheap, since they need to be run many times, but they also need to be representative for the processes to be described by the GMD. Considering the critical role of the interactions in wave growth, test cases first and foremost need to focus on wave growth, including effects of turning winds or winds not aligned with the waves. Swell mostly needs to be considered in the context of interactions between wind seas and swell. With this in mind, six deep water test cases have been designed, as summarized in Table 1. Additional shallow water tests are discussed in Tolman (2010a). Note that all tests produce a set of spectra from which arbitrary test parameters and metrics can be produced, as will be discussed in Sections 2.2 and 2.3.

Tests 01 and 02 represent conventional time- and fetch-limited growth curve computations. Test 01 considers 48 h of wave growth for a wind speed at 10 m height $U_{10} = 20 \text{ ms}^{-1}$. Initial conditions consist of a JONSWAP spectrum (Hasselmann, 1973) with peak frequency $f_p = 0.25 \text{ Hz}$ aligned with the wind. Forty-eight hourly spectra are saved for model comparison starting with the 1 h forecast. Test 02 considers the same initial conditions and wind speed blowing perpendicularly offshore from a straight coastline. The spatial model resolution is 10 km, and 50 spectra are saved at 10 km intervals starting 10 km offshore. Data are saved only at the end of 24 h of model integration. The width of the area considered is 500 km.

Test 03 is the ‘homogeneous front’ test of Tolman (1992). In a one-point model without propagation, initial conditions are set as in the previous tests. For four hours, a wind of $U_{10} = 10 \text{ ms}^{-1}$

is aligned with the initial wave conditions. For the next two hours the wind increases to $U_{10} = 20 \text{ ms}^{-1}$ while turning 90° . The wind then stays constant for 6 h, after which it linearly reduces to $U_{10} = 10 \text{ ms}^{-1}$ over the next 12 h, without changing direction. Forty-eight spectra are saved at 30 min intervals during the 24 h of model integration.

Test 04 is a one-point model with a continuously rotating wind. Initial conditions are set as in test 01, and the wind rotates continuously at a rate of $40^\circ/6 \text{ h}$. The slow rotation is used to assure that the spectrum stays unimodal. Integration is performed for 24 h, and 48 spectra are saved at 30 min intervals. Tests 03 and 04 deal with turning winds, where interaction approximations are known to influence results (e.g., Van Vledder and Holthuijsen, 1993).

Tests 05 and 06 are variations on tests 02 and 01, respectively. Test 05 is a slanting fetch case with winds under an angle of 45° with the coast. Except for the wind direction and the width of the basin (increased to 1000 km), this test is identical to test 02. In test 06 a narrow banded swell field with a wave height $H_s = 5 \text{ m}$ and peak frequency $f_p = 0.06 \text{ Hz}$ encounters the wind sea at an angle of 135° in a test that is otherwise identical to test 01. Both represent well known conditions where interaction parameterizations may be important (e.g., Ardhuin et al., 2007).

2.2. Test parameters

All test cases presented in the previous section produce wave spectra, for baseline reference runs using the exact WRT algorithm, and for the GMD with various parameter settings. Error measures could simply be based on the spectra directly, but this does not allow for optimizing more targeted behavior of the model. For the latter purposes, parameters computed from the spectrum will be defined first, after which associated error measures are defined in the following section.

Several classes of wave parameters can be distinguished. First, mean wave parameters identify bulk wave model behavior such as total energy generated and mean direction and speed of wave propagation. Considering such model parameters in the optimization allows for a strong constraining of mean model behavior, without which details in spectral model behavior may be irrelevant. Second, one-dimensional spectral measures, i.e., spectral measures based on integrating over spectral directions are important for many physical processes such as computation of

Table 1
Test cases.

Case	Description	Type	Spectra
01	Time-limited growth curve	1 point model	48
02	Fetch-limited growth curve	Quasi-stationary	50
03	Turning wind representing front	1 point model	48
04	Continuously turning wind	1 point model	48
05	Slanting fetch with offshore wind	Quasi-stationary	50
06	Wave growth with background swell	1 point model	48

wave-induced wind stresses and parameters relevant for remote sensing such as the mean squared slope. Finally, full spectral parameters and error measures are important to get all details of the model behavior optimized.

Mean wave parameters considered here are the significant wave height H_s , peak frequency f_p , mean direction $\bar{\theta}$ and directional spread σ_θ

$$H_s = 4\sqrt{m_0}, \quad m_0 = \iint F(f, \theta) df d\theta, \quad (10)$$

$$\bar{\theta} = \text{atan}\left(\frac{b}{a}\right), \quad (11)$$

$$\sigma_\theta = \left[2 \left\{ 1 - \left(\frac{a^2 + b^2}{m_0^2} \right)^{1/2} \right\} \right]^{1/2}, \quad (12)$$

$$a = \iint \cos(\theta) F(f, \theta) d\sigma d\theta, \quad (13)$$

$$b = \iint \sin(\theta) F(f, \theta) d\sigma d\theta, \quad (14)$$

and where f_p is determined by fitting a parabola to the peak of the one-dimensional spectrum $F(f)$.

$$F(f) = \int F(f, \theta) d\theta. \quad (15)$$

Note that such mean parameters can be computed for either the entire spectrum, or for individual spectral partitions representing wind sea and swell as occur in test 06 (e.g., Hanson et al., 2009).

Eq. (15) also represents the first of the one-dimensional spectral parameters. The energy spectrum focuses naturally on the behavior of the spectral peak. Many physical processes are governed by the behavior of the spectrum for frequencies above the spectral peak (including the spectral tail), which is more conveniently addressed by the steepness spectrum $G(f)$. Similarly, the behavior of the actual source terms should be addressed, even in a holistic optimization approach. This adds two more one-dimensional spectral parameters to be considered,

$$G(f) = k^2 F(f), \quad (16)$$

$$S_{nl}(f) = \int S_{nl}(f, \theta) d\theta. \quad (17)$$

Other relevant one-dimensional spectral parameters are the mean directions $\bar{\theta}(f)$ and directional spread $\sigma_\theta(f)$ as a function of spectral frequency, obtained by applying Eqs. (11) and (12) for each discrete spectral frequency band individually. Several additional parameters describe relevant aspects of the one-dimensional spectra and source term. One of such is the energy level in the high-frequency equilibrium range of the spectrum α , (Phillips, 1958), computed as

$$\alpha = (2\pi)^4 g^{-2} F(f) f^5, \quad (18)$$

which can be evaluated locally at the highest discrete frequency of the model. Similarly, the behavior in the transition range from spectral peak to equilibrium range can be evaluated in terms of level, power law fit or general fit to the reference model results (denoted here as “ β ”). A final relevant parameter from the source term is defined from the energy flux in frequency space $M(f)$

$$M(f) = \int_0^f S_{nl}(f_i) df_i. \quad (19)$$

This flux generally has a two-lobed structure, and the zero-flux frequency f_0 for which $M(f_0) = 0$ is important as it identifies a natural

separation of the spectrum into two parts which on average do not exchange energy.

Finally, the full two-dimensional spectrum $F(f, \theta)$, the corresponding steepness spectrum $G(f, \theta) = k^2 F(f, \theta)$ and the full interactions $S_{nl}(f, \theta)$ are considered.

2.3. Metrics

From the test parameters defined in the previous section, test metrics can be constructed. To consistently combine different error metrics, all metrics are normalized to become fractions or percentages. Normalization is, furthermore, applied locally in time (space) to assure equal weight for relative errors in all stages of development for each test. For instance, the wave height error is addressed locally as

$$\frac{H_{s,p} - H_{s,b}}{H_{s,b}}, \quad (20)$$

where the indices p and b represent the results from runs made with the parameterization (GMD) and the baseline computations (WRT), respectively. With N test spectra for an individual test case, the wave height error ϵ_H for the test case is defined as a conventional rms error

$$\epsilon_H = \sqrt{\frac{1}{N} \sum \left(\frac{H_{s,p} - H_{s,b}}{H_{s,b}} \right)^2}. \quad (21)$$

All other errors are defined similarly, and are presented in Appendix A. This results in fifteen individual error measures up from the five used in Tolman et al. (2004). Errors for all parameters and all test cases for the traditional DIA are presented as a baseline in Table 2. Whereas the DIA shows moderate errors for the four mean wave parameters, α and f_0 , large errors are found for all error measures based on one- or two-dimensional spectral data, consistent with known shortcomings of the DIA.

For each individual test case, these errors are combined into a single error measure

$$\epsilon_{nn} = \sum \epsilon_p a_p / \sum a_p, \quad (22)$$

where nn represent the number of the test from Section 2.1, ϵ_p represent the 15 error measures, and a_p represent corresponding weights, with a focus on (large weight for) mean wave parameters, as these are typically the primary output parameters of operational

Table 2

Individual parameter errors in percent of the traditional DIA relative to the exact (WRT) approach for all test cases. Two values for the first four error measures for test 06 indicate errors for wind sea and swell separately.

	Test case						
	01	02	03	04	05	06	
ϵ_H	15.4	13.9	9.1	8.9	11.7	16.1	5.5
ϵ_{fp}	5.4	6.0	2.1	2.8	5.1	5.8	0.8
$\epsilon_{\bar{\theta}}$	0.0	0.0	2.3	3.6	4.1	0.1	1.6
$\epsilon_{\bar{\sigma}}$	11.4	13.1	10.8	10.5	19.8	11.0	21.1
ϵ_α	9.4	6.4	15.9	17.1	9.1	10.0	
ϵ_{f_0}	2.0	3.3	4.1	7.0	5.0	2.5	
ϵ_β	70.0	61.0	60.6	62.8	64.2	70.8	
ϵ_{F1}	151	146	117	119	115	145	
ϵ_{G1}	80.3	76.1	63.5	64.5	62.9	81.1	
ϵ_{nl1}	87.8	89.7	81.8	83.5	65.0	88.5	
ϵ_θ	0.1	18.1	18.1	25.8	34.0	26.3	
ϵ_σ	46.3	40.7	45.9	48.5	56.0	43.4	
ϵ_{F2}	138	133	109	116	133	132	
ϵ_{G2}	59.5	58.0	56.5	58.7	60.2	60.0	
ϵ_{nl2}	87.5	89.3	81.6	82.2	74.6	88.2	

Table 3

Error weights in Eq. (22) as used in the optimization procedure for all test cases. Two values for test 06 indicate weights for wind sea and swell separately.

	Test case					
	01	02	03	04	05	06
ϵ_H	10	10	10	10	10	5 5
ϵ_{fp}	5	5	5	5	5	2.5 2.5
$\epsilon_{\bar{\theta}}$	5	5	5	5	5	2.5 2.5
$\epsilon_{\bar{\sigma}}$	5	5	5	5	5	2.5 2.5
ϵ_x	5	5	5	5	5	5
ϵ_{f0}	3	3	3	3	3	3
ϵ_{β}	3	3	3	3	3	3
ϵ_{F1}	1	1	1	1	1	1
ϵ_{G1}	1	1	1	1	1	1
ϵ_{nl1}	1	1	1	1	1	1
ϵ_{θ}	1	1	1	1	1	1
ϵ_{σ}	1	1	1	1	1	1
ϵ_{F2}	1	1	1	1	1	1
ϵ_{G2}	1	1	1	1	1	1
ϵ_{nl2}	1	1	1	1	1	1

wave models. Weights as used in this study are presented in Table 3. Finally, the total error metric for all test cases is computed as

$$\epsilon_{\text{tot}} = \sum \epsilon_{nn} b_{nn} / \sum b_{nn}, \quad (23)$$

where b_{nn} are the corresponding relative weights. In the present study, all weights of tests used in each optimization experiment are set equal ($b_{nn} \equiv 1$).

3. Genetic optimization

A DIA or GMD requires optimization of its free parameters. For the DIA, only two free parameters exist (λ, C), and all error measures for all tests can be addressed by direct mapping of errors in the two-dimensional parameter space, requiring typically $O(10^3)$ model runs for each test. Examples of error mapping for this configuration of the GMD, optimizing λ and C_{deep} for a single representative quadruplet, are presented in Fig. 1. Fig. 1a presents the total error ϵ_{tot} for all tests and all parameters in (λ, C_{deep}) space. A broad but well defined region exists with near-optimum model behavior (i.e., near-minimum errors). Fig. 1b shows that the corresponding minimum errors for individual parameters do not coincide in parameter space, and hence cannot be optimized simultaneously.

Another natural approach to optimizing (λ, C_{deep}) is using a steepest descent algorithm. In such an approach, a single first guess of the optimum value of (λ, C_{deep}) is made either randomly, or based on previous experience. From this location in parameters space a path to the location of the minimum error is sought by numerically evaluating partial derivatives of the error in parameter space, and following a path of steepest descent to the (local) error minimum. This requires absence of local minima and well-behaved derivatives of the model error in parameter space. For the simple DIA configuration of the GMD, steepest descent algorithms proved reasonably successful, although local rather than absolute error minima were found based on actual initial guesses of (λ, C_{deep}) (see Fig. 1b).

As will be shown below, an accurate GMD configuration for deep water can consist of as many as $n_{q,d} = 5$ representative quadruplets with four free parameters each ($\lambda, \mu, \theta_{12}, C_{\text{deep}}$), or 20 free parameters. Brute force mapping of errors in parameter space for this configuration may require as many as $O(10^{30})$ model runs per test case,³ which is obviously not feasible. Initial experiments

with steepest descent methods were also unsuccessful for such GMD configurations (Tolman et al., 2004; Tolman, 2005), due to the abundance of local minima in parameter space, and occasional near-discontinuous behavior of errors. However, the latter papers also introduced genetic optimization approaches as a feasible alternative to optimize parameters in a precursor to the GMD.

Genetic algorithms are loosely based on principles of natural selection, and genetic algorithms form a subset of what is generally identified as Evolutionary Computing (e.g., Eiben and Smith, 2003). A qualitative description of genetic optimization will be given in this section, introducing essential concepts and terminology. A detailed description of the algorithms developed for the optimization of the GMD is given in Appendix B. A software package to perform the genetic optimization is described in Tolman (2010b), and is intended for distribution with the next public release of WAVEWATCH III.

A genetic optimization approach starts with a sparse (typically random) sampling of the parameter space. For each sample the model error ϵ_{tot} is evaluated, and the samples are sorted with respect to the error. After the first sampling, the parameter space is re-sampled, using error information from the previous sampling in ways similar to natural selection in biology, as will be discussed in some more detail below. Re-sampling is repeated until a target accuracy or convergence is reached. Individual samplings of parameter space are called *populations* with individual *members*. Consecutive populations are called *generations*.

This process is illustrated in Fig. 2 with several generations of a genetic optimization of λ and C_{deep} in the GMD configuration corresponding to the traditional DIA. Each generation samples the parameter space with 50 members, compared to 806 combinations of (λ, C_{deep}) evaluated for error mapping of a sub-set of this space in Fig. 1a. In Fig. 2 individual members of the population are color coded according to their rank in the population based on their error ϵ_{tot} (rank 1 corresponds to the smallest error in the population). The corresponding error can be inferred from Fig. 1a.

The first generation (Fig. 2a) randomly samples parameter space. In the third generation (Fig. 2c) the highest ranked generations (blue colors) start to cluster around the absolute error minimum in Fig. 1a. In the tenth generation (Fig. 2f) the 20 highest ranked members of the population all virtually coincide with the optimum model configuration. In this case five generations, requiring the evaluation of 250 configurations, are sufficient to find the (near-) optimum GMD configuration. This is only moderately cheaper than full mapping of errors in parameter space. For more complex configurations, however, the reduction of effort between mapping and genetic optimization becomes dramatic, as will be shown in the following section.

The key feature of a generic optimization approach is the development of a new generation from the previous generation. This is where the link to natural selection in evolutionary biology arises. Members of the new generation are constructed from the previous generation by combining information from existing members of the previous generation. Pairs of such members from the previous generation (denoted as *parents*) are randomly selected with a higher probability of selection for members with smaller model errors. From a pair of *parents* from the previous generation, a pair of *children* in the new generation are generated by (i) mixing GMD configuration information from both parents (corresponding to genetic *cross-over recombination* in biology), and (ii) by randomly modifying the GMD configuration of the children (corresponding to genetic *mutation* in biology). The selection of *parents* and generation of *children* continues until the desired size of the new population is reached. To assure that the new generation includes the best configurations from the previous generation, some of these may be retained directly in the new generation (although this is not essential). This genetic optimization algorithm is illustrated in Fig. 3 and technical details are presented in Appendix B. Note that

³ Assuming that approximately $10^{1.5}$ realizations per parameter need to be evaluated for accurate mapping.

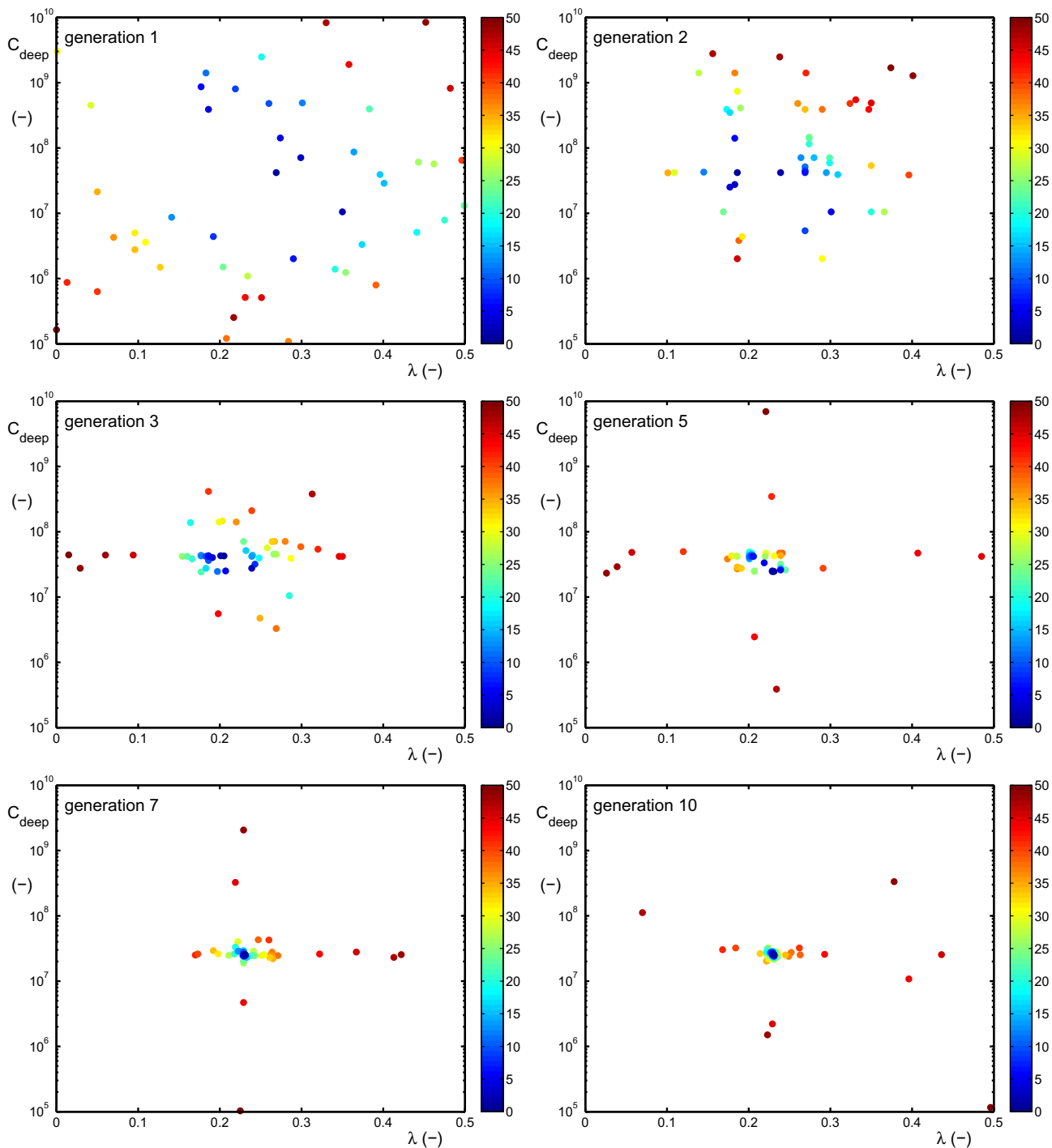


Fig. 2. Example evolution of generations for optimization of traditional DIA configurations. Color represents rank number in population, with rank 1 corresponding to smallest error. Corresponding overall model errors can be obtained from Fig. 1a.

the genetic approach does not rely on gradients of the error in parameter space, and hence can deal with discontinuities of errors in parameter space. Note, furthermore, that the re-sampling of parameter space for each consecutive generation implies that the algorithm does not automatically focus on identified local error minima, but can ‘jump’ between local error minima in parameter space.

Several additional considerations are important for genetic optimization in general.

First, continued convergence of a genetic algorithm relies on a broad set of parameter settings to be present in the parents (de-

noted as *diversity* in biology). Rapid initial convergence may lead to rapid loss of diversity, and hence poor final convergence. Conversely, slow initial convergence may lead to sustained diversity and better final convergence. As rapid initial convergence is often associated with large population sizes, and lack of diversity with small population sizes, the choice of the population size is important. As there are no clear guidelines for population sizes, this becomes an important (iterative) aspect of designing the genetic optimization experiments.

Second, convergence of genetic optimization algorithms is notoriously discontinuous; with no improvement between subsequent

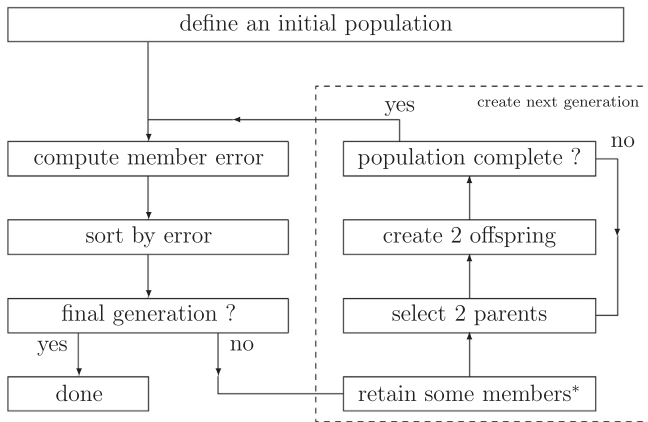


Fig. 3. General layout of a genetic search algorithm (*: optional).

generations intermixed with large improvements. Hence, the number of generations to be considered is typically selected manually, without introducing automated convergence criteria.

Third, genetic optimization is known to be efficient in getting near-optimum solutions, but is not as efficient in converging on the actual (local) error minimum. For this reason, a steepest descent method is always applied starting from the best performing member of the last generation (in literature denoted as an evolutionary hybrid method). This is done to assess the level of convergence of near-optimum solutions, and to address final convergence to a (local) minimum error in parameter space (see also previous point).

Fourth, with its random initialization, and random selection of parents and generation of children, the genetic optimization can be interpreted as a directed random search. Combined with the occurrence of many near-optimum solutions for complex GMD configurations (Tolman et al., 2004), it is therefore prudent to repeat the optimization experiments with different initial conditions. Here, three separate initial conditions are used for each experiment, for convenience denoted below as the ‘red’, ‘green’, and ‘blue’ experiments, consistent with colors used in subsequent figures.

4. Results

The GMD is foremost intended to provide an economical yet accurate nonlinear parameterization for operational wave models. This implies that the cheapest (i.e., least complex) configurations are preferable. Furthermore, only limited experience exists with genetic optimization of the GMD. Such experience is also best built by going to incrementally more complex configurations, until no more benefit in accuracy is gained, or the optimization becomes economically unfeasible. Furthermore, the present study focuses on establishing the genetic optimization approach described here, and less on the resulting GMD configurations. In this context, it is sufficient to establish the optimization for deep water only. The behavior of the resulting GMD configurations, including those optimized for shallow water, is discussed in detail in the companion paper (Tolman, accepted for publication).

The simplest possible configuration of the GMD is equivalent to the DIA configuration, i.e., using one quadruplet, defined by λ and C_{deep} only. This configuration was already used in the previous section to illustrate the features of genetic optimization. The evolution of generations as shown in Fig. 2 for a population size $n_{\text{pop}} = 50$ indicates that convergence is achieved after $n_{\text{gen}} = 5$ generations.

In general convergence can be estimated by assessing the evolution of the minimum error (ϵ_{min}) and the average error (ϵ_{avg} , here

defined for the fittest half of the population), as a function of the generation number. Convergence is associated with the minimum errors remaining unchanged with progressing generations, while the average error becomes close to the minimum error. Fig. 4 shows the evolution of these errors for the red, green and blue experiments, where the results presented in Fig. 2 correspond to the red experiment.

The red lines in Fig. 4 indicate that this experiment loses diversity after about five generations ($\epsilon_{\text{avg}} \approx \epsilon_{\text{min}}$, compare dashed and solid red lines; consistent with Fig. 2), and that no gain in accuracy is obtained with additional generations. The green experiment has a better initial conditions with smaller minimum and average errors than the red experiment, but requires more generations to reach the optimum solution and to lose diversity ($n_{\text{gen}} = 8-9$). Finally, the blue experiment combines the best initial conditions with quickly reaching the optimum error, while still retaining limited diversity in the last generation (ϵ_{avg} visibly above ϵ_{min} for the last generation, compare dashed and solid blue lines). Based upon this figure, it appears that $n_{\text{pop}} = 50$ and $n_{\text{gen}} = 10$ represent an adequate setup for this optimization experiment.

The DIA configuration of the GMD has been used above to illustrate how genetic optimization works, and that this technique indeed can find near-optimum configurations of the GMD. The next step is to increase the complexity of the GMD configuration by adding representative quadruplets, and by considering two- and three-parameter quadruplet definitions.

Population sizes (n_{pop}) were obtained by trial and error, increasing sizes slightly faster than linearly with the degrees of freedom of the optimization process. For the three-parameter quadruplet a larger random initial population was used to produce sufficient viable initial configurations (i.e., sufficient initial diversity).

The number of generations (n_{gen}) was determined interactively, using error evolution analysis as presented in Fig. 4. For the relatively cheap optimization experiments for the one-parameter quadruplet definition a liberal number of generations was used. For the more complex definitions n_{gen} was limited more aggressively, relying on the subsequent steepest descent optimization to guarantee (local) convergence.

Resulting experiment designs are presented in Table 4. Note that the two- and three-parameter quadruplet definitions

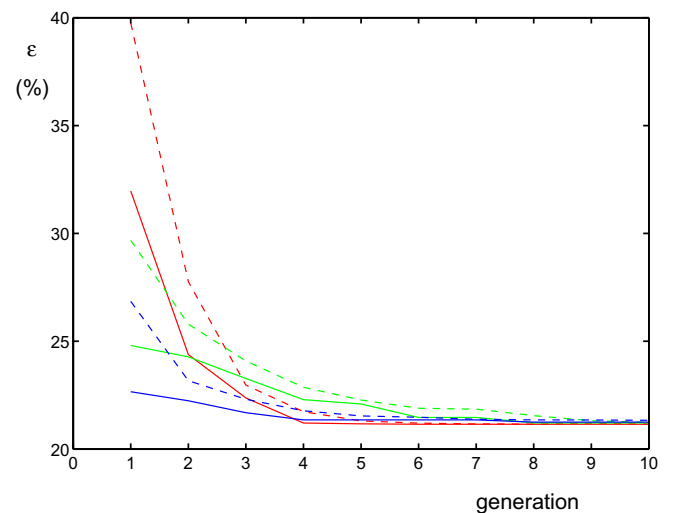


Fig. 4. Evolution of minimum error ϵ_{min} (solid lines) and average error ϵ_{avg} (dashed lines) as a function of the generation number. Traditional one-parameter DIA quadruplet configuration with $n_q = 1$ quadruplets. Red, green and blue lines represent the corresponding three experiments with different random initial conditions. (For interpretation of the references to colour in this figure legend, the reader is referred to the web version of this article.)

Table 4

Population sizes (n_{pop}) and number of generations (n_{gen}) for optimization experiments for one-, two- and three-parameter quadruplet definitions with n_q representative quadruplets. Population sizes in parentheses identify size of initial generation if different from subsequent population sizes.

n_q	(λ)		(λ, μ)		$(\lambda, \mu, \theta_{12})$	
	n_{pop}	n_{gen}	n_{pop}	n_{gen}	n_{pop}	n_{gen}
1	50	10	–	–	–	–
2	125	40	–	–	–	–
3	200	70	350	45	600 (1200)	60
4	350	100	500	60	1200 (2400)	60
5	–	–	600	60	1500 (3000)	90
6	–	–	750	60	2000 (4000)	150

Table 5

Minimum errors in percent for all deep water tests for various GMD configurations. DIA represent the WAVEWATCH III model with default DIA implementation. Error for one-, two- and three-parameter quadruplet definition.

n_q	Configuration		
	(λ)	(λ, μ)	$(\lambda, \mu, \theta_{12})$
DIA	25.1	–	–
1	21.2	–	–
2	16.5	–	–
3	15.7	14.2	11.9
4	15.6	11.9	11.2
5	–	11.0	9.25
6	–	10.8	9.08

generally require $n_q > 2$ for stable model integration, and are, therefore, not evaluated for $n_q \leq 2$. The corresponding total model errors ϵ_{tot} are presented in Table 5. The top line in the latter table represents the error for the WAVEWATCH III model with default DIA implementation as a baseline for improvements gained by adopting the GMD.

Table 5 shows a systematic reduction of the error with both an increased number of quadruplets n_q , and with the increased complexity of the quadruplet definition. For the one-parameter (λ) quadruplet definition improvement of the model error saturates when more than 3 or 4 representative quadruplets are considered, consistent with previous findings of Hashimoto and Kawaguchi (2001) and Van Vledder (2005). This will be discussed in more detail below. For the two-parameter (λ, μ) and three-parameter ($\lambda, \mu, \theta_{12}$) quadruplet definitions similar saturation appears to occur for $n_q = 5$ or 6. The reduced model error also results in qualitatively improved model behavior, as discussed in Tolman (accepted for publication).

To illustrate the power of genetic optimization for this problem, consider the optimization of the three-parameter quadruplet definition with $n_q = 5$ representative quadruplets. For this configuration, five sets of parameters $\lambda, \mu, \theta_{12}$ and C_{deep} need to be optimized, for a total of 20 free parameters. As mentioned above, brute force optimization would require $O(10^{30})$ configurations to be evaluated, which is economically unfeasible. Also, steepest descent methods have been shown to be incapable of producing near-optimum parameter estimates for such a configuration. The corresponding genetic optimization experiment as outlined in Table 4, however, requires the evaluation of only 1.310^5 configurations per random initial conditions to produce well-optimized parameter settings. Although this represents a serious computational effort, it is economically feasible even on moderately big cluster computers.⁴ Hence, genetic optimization is an astounding factor 10^{24} more effective than brute force optimization, and becomes an essential part of the development of the GMD.

Table 6

Optimum GMD configurations using traditional representative quadruplet definition and $n_q = 3$ representative quadruplets. i_q is quadruplet number sorted by λ . Red green and blue experiments with different random initial conditions.

	$i_q = 1$		$i_q = 2$		$i_q = 3$		ϵ_{tot}
	λ	C_{deep}	λ	C_{deep}	λ	C_{deep}	
Red	0.066	$5.80 \cdot 10^7$	0.184	$4.32 \cdot 10^7$	0.318	$1.43 \cdot 10^7$	16.0
Green	0.126	$4.79 \cdot 10^7$	0.237	$2.20 \cdot 10^7$	0.319	$1.10 \cdot 10^7$	15.7
Blue	0.066	$5.63 \cdot 10^7$	0.184	$4.33 \cdot 10^7$	0.318	$1.44 \cdot 10^7$	16.0

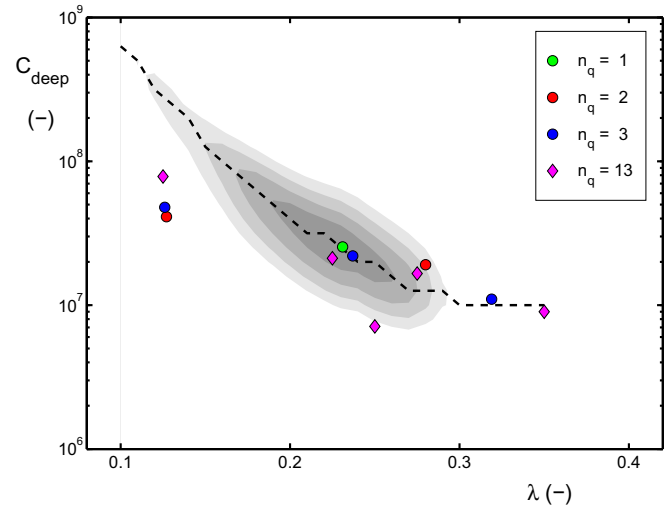


Fig. 5. Optimum deep water configurations for GMD using the traditional one-parameter quadruplet definition from the DIA. Shaded areas are obtained from error mapping from Fig. 1 with contours at 10% intervals above minimum error. Dashed line identifies optimum $C_{deep}(\lambda)$ from the mapping experiment. $n_q = 1-3$ results obtained by optimizing both λ and C_{deep} . $n_q = 13$ results obtained by sampling spectral space with 13 preset values of λ and optimizing the corresponding values for C_{deep} , resulting in $n_q = 5$ contributing quadruplets.

The remainder of the results section will illustrate some relevant aspects of the genetic optimization of GMD configurations. These illustrations will address the random and near-optimum nature of the results, saturation of improvements, and additional peculiarities of genetic optimization.

Genetic optimization techniques were selected to deal with multiple local near-minima of errors in parameter space. Furthermore, due to its random nature, the optimization with various initial conditions is expected to result in different near-optimum solutions. This is illustrated here with optimum parameter settings for the traditional one-parameter quadruplet definition with $n_q = 3$ representative quadruplets in Table 6. Here, the red and blue experiments result in virtually identical configurations, indicating the reproducibility of genetic optimization from different initial conditions. However, the green experiment produces a clearly different configuration with a clearly smaller total error. This indicates that reproduction of configurations from different initial conditions is no guarantee that this is the best overall solution, and that it is essential to repeat the experiments with multiple initial conditions. For more complex configurations, even more near-optimum solutions with less replication of configurations are found (resulting configurations not presented here).

The diminished improvement of the total error with increasing number of representative quadruplets suggests limitations of the accuracy of the GMD. This was already observed for the traditional DIA quadruplet layout by Van Vledder (2005), and attributed to an effective saturation of degrees of freedom in the parameterization

⁴ For the present experiments, typically 20–200 processors were used.

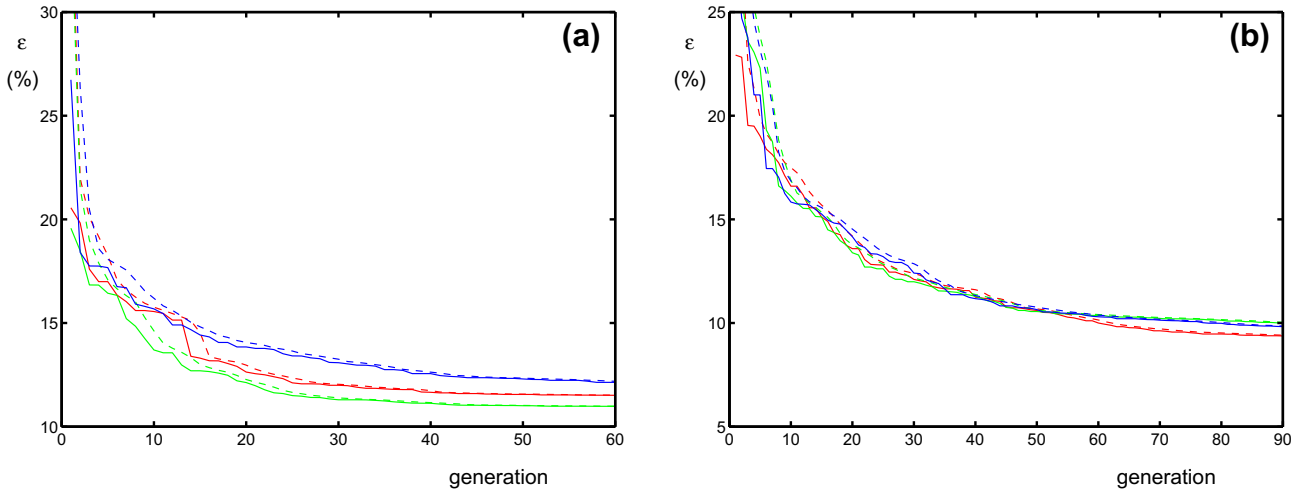


Fig. 6. Like Fig. 4 for experiments with (a) the two-parameter quadruplet definition and $n_q = 6$ representative quadruplets, and (b) the three-parameter quadruplet definition and $n_q = 5$ representative quadruplets.

Table 7

Like Table 6 for configuration using the two-parameter quadruplet definition and $n_q = 6$ representative quadruplets. Final error in percent estimated after complementary steepest descent optimization.

i_q	Red $\epsilon_{\text{tot}} = 11.47$			Green $\epsilon_{\text{tot}} = 10.97$			Blue $\epsilon_{\text{tot}} = 10.78$		
	λ	μ	C_{deep}	λ	μ	C_{deep}	λ	μ	C_{deep}
1	0.098	–	$5.27 \cdot 10^7$	0.069	0.045	$7.41 \cdot 10^8$	0.059	0.026	$2.59 \cdot 10^8$
2	0.123	0.092	$4.43 \cdot 10^8$	0.183	0.002	$5.39 \cdot 10^7$	0.132	0.080	$2.60 \cdot 10^8$
3	0.182	0.120	$8.75 \cdot 10^5$	0.232	0.147	$5.95 \cdot 10^7$	0.227	0.127	$6.30 \cdot 10^7$
4	0.232	0.068	$5.47 \cdot 10^7$	0.233	0.064	$1.22 \cdot 10^7$	0.279	–	$1.36 \cdot 10^7$
5	0.328	0.145	$2.54 \cdot 10^7$	0.278	0.237	$1.44 \cdot 10^7$	0.351	0.219	$1.47 \cdot 10^7$
6	0.383	–	$2.37 \cdot 10^6$	0.351	0.110	$1.92 \cdot 10^7$	0.359	0.070	$7.03 \cdot 10^6$

in spite of a further increase of the number of representative quadruplets n_q .

To assure that this ‘saturation’ is not an artifact of the genetic optimization, an additional optimization experiment has been performed with the one-parameter quadruplet layout. In this experiment $n_q = 13$ quadruplets are considered with pre-set values of λ ranging from 0.100 to 0.400 and increments of 0.025. The corresponding strengths C_{deep} were optimized using a population size of $n_{\text{pop}} = 500$ and considering $n_{\text{gen}} = 40$ generations. It was found that no more than 5 of the 13 quadruplets contributed to the solution, with a resulting optimum model error $\epsilon_{\text{tot}} = 15.9\%$. This clearly indicates that the saturation of improvement with increase of the number of quadruplets is a feature of the GMD, and not a feature of the optimization.

Fig. 5 summarizes the optimization results for traditional DIA quadruplet definition with multiple representative quadruplets. The shaded area and dashed line in this figure represent the results of the mapping experiments, with the genetic optimization results for $n_q = 1$ (green square) centered on the shaded area as expected. The figure shows that there are favored quadruplet configurations used by multiple GMD configurations. It also shows that optimized quadruplets do not have strengths C_{deep} much larger than found in mapping for the given λ , but can be smaller by up to an order of magnitude. If C_{deep} becomes much smaller than that, the resulting quadruplet does not contribute to the model results. It is then either removed automatically by the optimization, or can be removed by hand without influencing the model error (see Tolman, 2010a).

Finally, Fig. 6 shows error evolutions for optimization experiments for two configurations, and Table 7 show the optimization results corresponding to Fig. 6a. These experiments have been chosen to illustrate peculiarities of the genetic optimization, augmented with a steepest descent algorithm.

Fig. 6a and Table 7 present results for the optimization of a GMD configuration using the two-parameter quadruplet definition with $n_q = 6$ representative quadruplets. Typical behaviors for these experiments include: (a) clearly different near-optimum solutions, and (b) clearly different error evolutions, both indicating the need for performing the optimization with a variety of initial conditions. (c) Table 7 illustrates the occurrence of degenerated quadruplets with $\mu = 0$. In this case the two-parameter quadruplet becomes a one-parameter quadruplet. (d) In the red experiment quadruplet $i_q = 3$ has an anomalously weak C_{deep} and is effectively switched off, resulting in a configuration with effectively $n_q = 5$.

This experiment illustrates two more behaviors of genetic optimizations. The first occurs for the red experiment. In generation 13, this experiment has prematurely focused on a non-optimum configurations, and has lost most of its diversity ($\epsilon_{\text{min}} \approx \epsilon_{\text{avg}}$). In generation 14, however, the minimum errors dramatically decrease and the diversity of the population increases. This shows that the experiment is able to focus on a more appropriate near-optimum solution and illustrates the capability of the genetic optimization procedure to ‘jump’ from one local minimum to another local error minimum in parameter space. The second behavior is observed when comparing the results for the blue experiment in Fig. 6a and Table 7; in the figure, the blue experiment shows the largest

final total error, whereas in the table it proves most accurate. This represents a situation where the final convergence of the genetic optimization was slow, and where a subsequent steepest descent algorithm resulted in a dramatic improvement of the error of the optimum configuration. This illustrates the usefulness of augmenting the genetic optimization with a steepest descent algorithm.

Fig. 6b shows the error evolution for a GMD configuration with the three-parameter quadruplet definition and $n_q = 5$ representative quadruplets. This configuration shows much more consistent error evolution between the three experiments with final optimum errors of the genetic optimization experiments of 9.37%, 9.99%, and 9.83%, respectively. The steepest descent optimization improved these errors to 9.25%, 9.31% and 9.83%, respectively, influencing the green experiment most. All three final configurations are clearly distinct, without displaying degenerate configurations (configurations not presented here).

5. Discussion and conclusions

The present study presents new objective optimization techniques for free parameters in a Generalized Multiple DIA parameterization of nonlinear interactions in wind waves (GMD, Tolman, accepted for publication). Key elements are the holistic and genetic nature of the optimization. It is shown that the most accurate GMD configurations require 20 or more free parameters to be optimized objectively.

Holistic optimization implies that full model integration results are optimized, using idealized test cases. For each test case baseline results are obtained with the exact nonlinear interactions computed using the Webb–Resio–Tracy (WRT) method. Results obtained with the GMD parameterization are compared to the baseline results using fifteen objective metrics computed from modeled wave spectra (48–50 spectra per test case). A similar approach was used subjectively by Hasselmann et al. (1985). The objective approach was (re-)introduced by Tolman et al. (2004). A companion paper (Tolman, accepted for publication) demonstrates that improved model behavior (smaller objective errors) for idealized test cases results in similar improvements in realistic applications. A more commonly used optimization approach, fitting interactions approximations for idealized spectra only, has no such guarantee (e.g., Tolman et al., 2004).

Traditional brute-force optimization is unfeasible for the optimization of a GMD with 20 or more free parameters due to the sheer number of configurations to be evaluated. Traditional steepest descent methods proved unsuccessful due to the occurrence of many local error minima in parameter space, and due to non-smooth derivatives of errors in parameter space (Tolman et al., 2004; Tolman, 2005). The latter papers also introduced genetic optimization as a feasible technique to objectively and simultaneously optimize a large number of free parameters in the GMD. The genetic optimization is further developed in the present study and presented in Sections 3 and Appendix B.

The genetic optimization techniques are applied to GMD configurations for deep water with increasing complexity (i.e., increasing numbers of free parameters). In these experiments, the following results and conclusions were obtained:

- (i) The genetic optimization procedure developed in the present study is capable of optimizing more than 20 free parameters in GMD.
- (ii) The method is highly efficient, as is evident in the fact that optimization of 20 parameters required $O(10^6)$ model evaluations, compared to $O(10^{30})$ model evaluations needed for brute force error mapping for such a GMD configuration. Note, furthermore, that the genetic optimization is highly

suitable for parallelization of computations, as errors for various members of the population can be computed in parallel (see Tolman, 2010b). The same holds true for error mapping, but generally not for steepest descent methods.

- (iii) Due to the inherently random nature of genetic optimization, it is essential to use an ensemble of optimization experiments for each GMD configuration considered. The ensemble size of three as used here is a bare minimum to assess the need and power of using an ensemble approach.
- (iv) The random nature of the optimization also results in finding multiple near-optimum solutions rather than the objectively single optimum solution. This implies that different near-optimum solutions can be found for different ensemble members.
- (v) An important feature of the genetic optimization is that the method allows for ‘jumping’ between local minima, so that the method does not ‘lock in’ on marginal local minima identified early in the process.
- (vi) Added complexity of a GMD configuration leads to added accuracy, both in terms of the complexity of definition of the representative quadruplet, and in terms of the number of representative quadruplets.
- (vii) Saturation of improvement occurs with adding complexity to the GMD configuration. For the traditional DIA quadruplet configuration, it has been shown that the saturation of improvements has occurred when approximately 4 or 5 representative quadruplets are considered, and that the saturation is a feature of the GMD and not of the optimization approach, consistent with previous results of Hashimoto and Kawaguchi (2001) and Van Vledder (2005). For more complex quadruplet configurations saturation also appears to occur, and is likely to also be associated with the GMD rather than the optimization approach.
- (viii) A hybrid method, adding a steepest descent approach starting from the best performing configuration of a given generation, helps to assess if convergence on the (local) error minimum is reached, and in some cases results in much better convergence on the error minimum.

In the present study, the optimization techniques are applied to deep water configurations of the GMD only. As shown in Tolman (2010a) the above conclusions equally hold for shallow water optimization, when adding appropriate shallow water test cases.

It should be noted that the other source terms used in the WAVEWATCH III model [see Eq. (1)] were not developed for the exact interactions, but explicitly for the DIA. It is not clear, whether the present GMD configurations can be considered as universal optimized configurations, or that the optimum configuration is dependent on the input and dissipation source terms. Until and unless universality of optimized configurations is demonstrated, it will be prudent to repeat GMD optimizations for other input and dissipation source term packages. Similarly, it is easy to add new test cases or new error parameters, to focus on specific behavior of the interactions. This would also require additional optimization experiments, which can be performed using the package developed for this study (Tolman, 2010b).

If the optimization of the GMD is repeated, lessons learned from the present study can be applied, for instance.

- (a) The saturation of improvement appears to be a feature of the GMD, related to inherent degrees of freedom. It should therefore be sufficient to concentrate on the one-parameter quadruplet definition with $n_q = 3$ or 4 representative quadruplets and the three-parameter quadruplet definition with $n_q = 5$ or 6 representative quadruplets.

- (b) Using ensembles of three optimization experiments for each configuration is a bare minimum. When a smaller number of configurations is considered it becomes more feasible to use a large variety of initial conditions. Note that an economic way of using a large ensemble would be to obtain partial convergence with a limited number of generations for a large ensemble, while assessing full convergence with sufficient populations only with the most promising of the initial ensemble members (similar to ‘island methods’, e.g., Eiben and Smith, 2003).
- (c) The development of an evolutionary optimization approach is part art and part science, with many subjective choices made along the way. Many of these choices could be considered in more detail in future studies. However, the present optimization approach has clearly been proven to be highly efficient for the highly nonlinear optimization required here, and it may be more effective to spend more effort on refining the GMD, than on further refining the optimization techniques.

Acknowledgments

The authors thank D.B. Rao and Stephen Lord for their long term support for the presented research at NCEP. The author thanks Vladimir Krasnopolsky, Henrique Alves, Will Perrie, and the anonymous reviewers for their input in early drafts of this manuscript. The present study was made possible by various funding sources from NOAA and from the Office of Naval Research (ONR).

Appendix A. Expressions for error metrics

Errors for the peak frequency (f_p, ϵ_{f_p}), mean direction ($\bar{\theta}, \epsilon_{\bar{\theta}}$), and directional spread ($\sigma_{\theta}, \epsilon_{\sigma}$) are defined as

$$\epsilon_{f_p} = \sqrt{\frac{1}{N} \sum_N \left(\frac{f_{p,p} - f_{p,b}}{f_{p,b}} \right)^2}, \quad (\text{A.1})$$

$$\epsilon_{\bar{\theta}} = \sqrt{\frac{1}{N} \sum_N \left(\frac{\bar{\theta}_p - \bar{\theta}_b}{\Delta\theta_n} \right)^2}, \quad (\text{A.2})$$

$$\epsilon_{\sigma} = \sqrt{\frac{1}{N} \sum_N \left(\frac{\sigma_{\theta,p} - \sigma_{\theta,b}}{\sigma_{\theta,b}} \right)^2}, \quad (\text{A.3})$$

where the normalization angle $\Delta\theta_n$ needs to be defined, since no natural normalization angle exists. Somewhat arbitrarily $\Delta\theta_n = 90^\circ$ is chosen here. In test 06 these errors are defined for the wind sea and swell separately. Errors for the high-frequency energy level ($\alpha, \epsilon_\alpha; \beta, \epsilon_\beta$) and the nonlinear zero-frequency (f_0, ϵ_{f_0}) are defined as

$$\epsilon_\alpha = \sqrt{\frac{1}{N} \sum_N \left(\frac{\alpha_p - \alpha_b}{\alpha_b} \right)^2}, \quad (\text{A.4})$$

$$\epsilon_\beta = \frac{1}{N} \sum_N \sqrt{\frac{\int_{1.5f_p}^{3.0f_p} [G_p(f) - G_b(f)]^2 df}{\int_{1.5f_p}^{3.0f_p} G_b(f) df}}, \quad (\text{A.5})$$

$$\epsilon_{f_0} = \sqrt{\frac{1}{N} \sum_N \left(\frac{f_{0,p} - f_{0,b}}{f_{0,b}} \right)^2}. \quad (\text{A.6})$$

Errors for the one-dimensional spectrum ($F(f), \epsilon_{F1}$), steepness spectrum ($G(f), \epsilon_{G1}$), and the source term ($S_{nl}(f), \epsilon_{nl1}$) are defined as

$$\epsilon_{F1} = \frac{1}{N} \sum_N \sqrt{\frac{\int_0^{f_2} [F_p(f) - F_b(f)]^2 df}{\int_0^{f_2} F_b(f) df}}, \quad (\text{A.7})$$

$$\epsilon_{G1} = \frac{1}{N} \sum_N \sqrt{\frac{\int_0^{f_2} [G_p(f) - G_b(f)]^2 df}{\int_0^{f_2} G_b(f) df}}, \quad (\text{A.8})$$

$$\epsilon_{nl1} = \frac{1}{N} \sum_N \sqrt{\frac{\int_0^{f_2} [S_{nl,p}(f) - S_{nl,b}(f)]^2 df}{\int_0^{f_2} S_{nl,b}^2(f) df}}. \quad (\text{A.9})$$

The upper integration bound $f_2 = 3.5f_p$ is explicitly defined to assure that errors in the parametric tail, which for $F(f)$ are constant, may not dominate the error measure, or that the integration range does not influence the results (as for $G(f)$). Here f_p is determined from the wind sea partition of the spectrum. The error measures for the spectral direction and spread ($\theta(f), \epsilon_\theta$ and $\sigma(\theta), \epsilon_\sigma$) are defined as

$$\epsilon_\theta = \frac{1}{N} \sum_N \sqrt{\frac{\int_{f_1}^{f_2} [\theta_p(f) - \theta_b(f)]^2 df}{\theta_n(f_2 - f_1)}}, \quad (\text{A.10})$$

$$\epsilon_\sigma = \frac{1}{N} \sum_N \sqrt{\frac{\int_{f_1}^{f_2} [\sigma_p(f) - \sigma_b(f)]^2 df}{\sigma_{\theta,1.2}(f_2 - f_1)}}. \quad (\text{A.11})$$

These directional parameters are defined even for spectral frequencies with virtually no energy. To assure that the error measure focuses on a spectral range containing energy only, f_1 and f_2 are chosen to only include frequencies for which $F(f) > 0.001F_{\max}$, where F_{\max} is the maximum energy of the corresponding spectrum. Finally, the errors for the two-dimensional spectral and source term errors are defined as

$$\epsilon_{F2} = \frac{1}{N} \sum_N \sqrt{\frac{\int_0^{2\pi} \int_0^{f_2} [F_p(f, \theta) - F_b(f, \theta)]^2 df d\theta}{\int_0^{2\pi} \int_0^{f_2} F_b(f, \theta) df d\theta}}, \quad (\text{A.12})$$

$$\epsilon_{G2} = \frac{1}{N} \sum_N \sqrt{\frac{\int_0^{2\pi} \int_0^{f_2} [G_p(f, \theta) - G_b(f, \theta)]^2 df d\theta}{\int_0^{2\pi} \int_0^{f_2} G_b(f, \theta) df d\theta}}, \quad (\text{A.13})$$

$$\epsilon_{nl2} = \frac{1}{N} \sum_N \sqrt{\frac{\int_0^{2\pi} \int_0^{f_2} [S_{nl,p}(f, \theta) - S_{nl,b}(f, \theta)]^2 df d\theta}{\int_0^{2\pi} \int_0^{f_2} S_{nl,b}^2(f, \theta) df d\theta}} \quad (\text{A.14})$$

with f_2 defined as with the corresponding one-dimensional spectral error measures.

Appendix B. Genetic optimization

This appendix presents relevant details of the genetic optimization techniques designed to optimize the free parameters of the GMD. The description of a single member of the population is discussed in Appendix B.1. For completeness, this also includes parameters for the strong or shallow water scaling, although actual optimization in such conditions is not addressed in this manuscript. Appendix B.2 describes the construction of the initial population, and Appendix B.3 describes the evolution of consecutive populations.

Table B.1

Basic description of members of a population: i_g is the sequence number of the parameter in the description; n_q is the number of representative quadruplets; i_q is the quadruplet number. Note that $\theta_{12} < 0^\circ$ is used to identify (one- or) two parameter quadruplet definitions. std and γ refer to perturbation mutation in Table B.2

i_g	Par.	Range	acc.	Type	Std
$5(i_q - 1) + 1$	λ	0–0.5	0.001	Lin	0.25γ
$5(i_q - 1) + 2$	μ	0–0.5	0.001	Lin	0.25γ
$5(i_q - 1) + 3$	θ_{12}	0–180°	0.1°	Lin	$45^\circ\gamma$
$5(i_q - 1) + 4$	C_{deep}	$10^5 - 10^{10}$	3 digit	Exp	γC_{deep}
$5(i_q - 1) + 5$	C_{shal}	$10^4 - 10^9$	3 digit	Exp	γC_{shal}
$5n_q + 1$	m	(–8) to 4	0.01	lin	$4 \cdot \gamma$
$5n_q + 2$	n	(–6) to (–2)	0.01	lin	$4 \cdot \gamma$

B.1. The genome

A population in the genetic optimization approach is characterized by its members and their ‘fitness’ (or error). In a traditional genetic optimization approach, and in the precursor to the present study (Tolman et al., 2004), an individual member of the population is represented by a bit string (e.g., Holland, 1992). For the present optimization problem, it is more natural to use a set of real numbers to describe a member of the population, which is commonly called an evolutionary strategy approach (Eiben and Smith, 2003).

The description of a member of the population needs to include the five free parameters of a representative quadruplet ($\lambda, \mu, \theta_{12}, C_{\text{deep}}, C_{\text{shal}}$) for each i_q of n_q representative quadruplets and the scaling parameters (m, n) from Eq. (1) through (9). This results in $n_g = 5n_q + 2$ numbers describing a member of the population, as outlined in Table B.1. For practical reasons, the population information is stored in human-readable formatted data files. This effectively creates an accuracy limit at which the parameters are described, as is documented in Table B.1. This Table also presents the allowed range of all parameters, based on physical limitations of parameters and on experiments with error mapping for single quadruplets. Note that invalid quadruplet configurations arising in the initialization or in children are not added to a population (corresponding to lethal mutation in biology).

Finally, a fitness value ζ is traditionally defined for each member of a population. The fitness is naturally defined here as the inverse of the model error

$$\zeta = \epsilon_{\text{tot}}^{-1}. \quad (\text{B.1})$$

Note that not all free parameters need to be optimized for a given GMD configuration. Therefore, a mask consisting of n_q logical values is defined for each optimization experiment, identifying which parameters are to be optimized. The population management techniques described below only modify GMD parameters that are thus identified, using preset (unchanging) values for all other parameters.

B.2. The initial population

The initial population is generated by a simple random initialization. For λ, μ and θ_{12} direct physical limitations of the parameter settings are available, as discussed in the previous section. For the initial population, values for these three parameters for each member are set randomly assuming a uniform distribution of values in the valid range of the parameter (Table B.1).

Allowed values of C_{deep} and C_{shal} are not naturally bounded and are set in a wide range around values expected from previous mapping and inverse modeling studies. Because these parameters cover several orders of magnitude, an exponential type of distribution is

used where $\log(C_{\text{deep}})$ and $\log(C_{\text{shal}})$ are uniformly distributed over their valid range.

Particularly for a GMD using the three-parameter quadruplet definition many less viable quadruplets are generated when a purely random initialization is used. This may result in too few viable quadruplets on which the optimization focuses too quickly, in effect limiting the diversity of the population. To avoid this, a larger number of random realizations may be considered to fill the first population, of which only the fittest members are retained.

B.3. Subsequent populations

When the initial population has been established, the fitness ζ of each member is computed, and the population is sorted by descending fitness. A population model is needed to populate the next generation (Eiben and Smith, 2003, Sections 3.6 and 8.8). In the present study, a small fraction of the best performing members of the population is retained. All other members of the new population are generated as offspring of parents from the previous population.

Only fit members of the present population are allowed to become parents, defined by their model error

$$\epsilon \leq X_p \epsilon_{\text{min}}, \quad (\text{B.2})$$

where ϵ_{min} is the error of the fittest member of the population. The resulting fraction of the population that is allowed to become parent is furthermore limited by a minimum and a maximum fraction of the population. With this, the limiting fitness (ζ_{lim}) is defined as the fitness of the fittest member of the population that is not allowed to become a parent, or, if l members of a ranked population are allowed to have offspring, $\zeta_{\text{lim}} = \zeta_{l+1}$. The probability p_i of each parent with index $i \leq l$ to be chosen as a parent is defined as

$$p_i = (\zeta_i - \zeta_{\text{lim}}) \left(\sum_{i=1}^l \zeta_i - \zeta_{\text{lim}} \right)^{-1}. \quad (\text{B.3})$$

Using these probabilities, sets of two parents are randomly selected until sufficient offspring has been generated.

The first step in the process of generating offspring from parents is cross-over recombination. Both parents are defined by a ‘string’ of $5n_q + 2$ real numbers. Randomly, 0, 1 or 2 crossover points are selected in this string. On one side of a crossover point, data is taken from parent one, on the other side, data is taken from parent two. When parents are described with bit strings rather than real numbers, the crossover point may be in the middle of the description of a physical parameter, hence ‘mixing’ information of both parents for that parameter.

In the simplest approach to mutation with real-valued parameters denoted as simple recombination in (Eiben and Smith, 2003, Section 3.5.3), all parameter values are directly taken from one of the two parents without additional considerations at the crossover point.

Another process denoted as single arithmetic recombination describes this process at the crossover point by taking a single parameter in the child, and defining it as a weighted average of the parameter values of the two parents. Defining the parents as x and y , the child as c , and the index i representing the crossover parameter value index, the parameter value of the first child is determined as

$$c_i = \kappa x_i + (1 - \kappa) y_i, \quad (\text{B.4})$$

and the parameter value for the second child is obtained by exchanging x and y . In the present algorithm, a random choice is made between simple and single arithmetic recombination, and κ is also chosen randomly.

Table B.2

Parameters used in the generation of children from parents in the genetic optimization procedure. See Table B.1 for computation of γ in perturbation mutation from spread parameter.

Fraction of old population retained	0.05
Error factor for parent selection (X_p)	2.00
Minimum parent fraction	0.25
Maximum parent fraction	0.50
Probability of 0 crossovers	0.50
Probability of 1 crossover	0.25
Probability of 2 crossovers	0.25
Probability of arithmetic recombination	0.50
Expected number of mutations	1.25
Probability of uniform mutation (otherwise perturbation mutation)	0.30
Spread parameter in perturbation (γ)	0.10

After recombination, the children are further changed from their parents by allowing for mutations, that is, random changes in one or more of the real numbers describing the child. An expected number of mutations per child is pre-described. Two types of mutation are considered. One is uniform mutation, where in effect the parameter to be mutated is randomly re-initialized. The second type is mutation by perturbation, where the parameter value is modified slightly, using a normal distribution with a small predefined standard deviation (identified by γ in Table B.1). Finally, mutations are capable of switching between one-, two-, or three-parameters quadruplet definitions, and to switch deep and/or shallow water scaling on or off. With an expected number of mutations per child set to approximately 1, many children will not have mutations.

Parameter settings for the genetic optimization scheme used here are gathered in Table B.2. Because there are no hard and fast rules for setting most parameters, their values have been based on common sense and numerical experimentation.

References

- Ardhuin, F., Herbers, T.H.C., Watts, K.P., Van Vledder, G.P., Jensen, R., Graber, H., 2007. Swell and slanting fetch effects on wind wave growth. *J. Phys. Oceanogr.* 37, 908–931.
- Eiben, A.E., Smith, J.E., 2003. *Introduction to Evolutionary Computing*. Springer, 299 pp.
- Hanson, J.L., Tracy, B.A., Tolman, H.L., Scott, R.D., 2009. Pacific hindcast performance of three numerical wave models. *J. Atmos. Oceanic Technol.* 26, 1614–1633.
- Hashimoto, N., Kawaguchi, K., 2001. Extension and modification of Discrete Interaction Approximation (DIA) for computing nonlinear energy transfer of gravity wave spectrum. In: 4th International Symposium on Ocean Wave Measurement and Analysis. ASCE, pp. 530–539.
- Hasselmann, K., 1960. Grundgleichungen der Seegangsvoraussage. *Schiffstechnik* 7, 191–195.
- Hasselmann, S., Hasselmann, K., Allender, J.H., Barnett, T.P., 1985. Computations and parameterizations of the nonlinear energy transfer in a gravity-wave spectrum, Part II: Parameterizations of the nonlinear energy transfer for application in wave models. *J. Phys. Oceanogr.* 15, 1378–1391.
- Hasselmann, K., Barnett, T.P., Bouws, E., Carlson, H., Cartwright, D.E., Enke, K., Ewing, J.A., Gienapp, H., Hasselmann, D.E., Kruseman, P., Meerburg, A., Müller, P., Olbers, D.J., Richter, K., Sell, W., Walden, H., 1973. Measurements of wind-wave growth and swell decay during the Joint North Sea Wave Project (JONSWAP). *Ergänzungsheft zur Deutschen Hydrographischen Zeitschrift, Reihe A(8)* 12, 95 pp.
- Holland, J.H., 1992. *Adaptation in Natural and Artificial Systems*. MIT Press, Cambridge, MA.
- Phillips, O.M., 1958. The equilibrium range in the spectrum of wind-generated waves. *J. Fluid Mech.* 4, 426–434.
- Resio, D.T., Perrie, W., 1991. A numerical study of nonlinear energy fluxes due to wave-wave interactions Part 1: Methodology and basic results. *J. Fluid Mech.* 223, 603–629.
- SWAMP Group, 1985. *Ocean Wave Modelling*. Plenum Press, 256 pp.
- Tolman, H.L., 1992. Effects of numerics on the physics in a third-generation wind-wave model. *J. Phys. Oceanogr.* 22, 1095–1111.
- Tolman, H.L., 2005. Optimum Discrete Interaction Approximations for wind waves. Part 2: Convergence of model integration. Tech. Note 247, NOAA/NWS/NCEP/MMAB, 74 pp. + Appendices.
- Tolman, H.L., 2008. Optimum Discrete Interaction Approximations for wind waves. Part 3: Generalized Multiple DIAs. Tech. Note 269, NOAA/NWS/NCEP/MMAB, 117 pp.
- Tolman, H.L., 2009. User Manual and System Documentation of WAVEWATCH III™ version 3.14. Tech. Note 276, NOAA/NWS/NCEP/MMAB, 194 pp. + Appendices.
- Tolman, H.L., 2010a. Optimum Discrete Interaction Approximations for wind waves. Part 4: Parameter optimization. Tech. Note 288, NOAA/NWS/NCEP/MMAB, 175 pp.
- Tolman, H.L., 2010b. A Genetic Optimization Package for the Generalized Multiple DIA in WAVEWATCH III™. Tech. Note 289, Ver. 1.0, NOAA/NWS/NCEP/MMAB, 21 pp.
- Tolman, H.L., Krasnopolsky, V.M., 2004. Nonlinear interactions in practical wind wave models. In: 8th International Workshop on Wave Hindcasting and Forecasting. JCOMM Tech. Rep. 29, WMO/TD-No. 1319, Paper E1.
- Tolman, H.L., accepted for publication. A Generalized Multiple Discrete Interaction Approximation for resonant four-wave nonlinear interactions in wind wave models with arbitrary depth. *Ocean Modell.*
- Tracy, B., Resio, D.T., 1982. Theory and Calculation of the Nonlinear Energy Transfer between Sea Waves in Deep Water. WES Report 11, US Army Corps of Engineers.
- Van Vledder, G.P., 2002. A Subroutine Version of the Webb/Resio/Tracy Method for the Computation of Nonlinear Quadruplet Interactions in a Wind-wave Spectrum. Report 151b, Alkyon, The Netherlands.
- Van Vledder, G.P., 2005. The triplet method for the computation of nonlinear four-wave interactions in discrete spectral wave models. In: Edge, B.L., Hemsley, J.M. (Eds.), 5th International Symposium on Ocean Wave Measurement and Analysis, ASCE, Paper 48.
- Van Vledder, G.P., 2006. The WRT method for the computation of non-linear four wave interactions in discrete spectral wave models. *Coastal Eng.* 53, 223–242.
- Van Vledder, G.P., Holthuijsen, L.H., 1993. The directional response of ocean waves to turning winds. *J. Phys. Oceanogr.* 23, 177–192.
- Webb, D.J., 1978. Non-linear transfers between sea waves. *Deep-Sea Res.* 25, 279–298.